Ramparts around Lakes on Titan Impact Winds and Methane Evaporation

Enora Moisan, Audrey Chatain, Scot Rafkin, Alejandro Soto, Shannon Mackenzie, Aymeric Spiga

The Planetary Science Journal, 6:220 (15pp), 2025 September https://doi.org/10.3847/PSJ/adf631

Ramparts around Lakes on Titan Impact Winds and Methane Evaporation

Enora Moisan[1,2,3], Audrey Chatain[1,4,5], Scot Rafkin[1], Alejandro Soto[1], Shannon MacKenzie[6], and Aymeric Spiga[3]
[1] Department of Space Studies, Southwest Research Institute (SwRI), Boulder, CO, USA
[2] ENS de Lyon, University of Lyon, CNRS, LGL-TPE, 46 Allée d'Italie, F-69007 Lyon, France
[3] Laboratoire de Météorologie Dynamique/Institut Pierre-Simon Laplace (LMD/IPSL), Centre National de la Recherche Scientifique (CNRS), Sorbonne Université, 4 place Jussieu, Tour 45-55 3e étage, 75252 Paris, France
[4] Departamento de Física Aplicada, Escuela de Ingeniería de Bilbao, Universidad del País Vasco/Euskal Herriko Unibertsitatea (UPV/EHU), Bilbao, Spain
[5] Laboratoire Atmosphères Observations Spatiales/Institut Pierre-Simon Laplace (LATMOS/IPSL), Université Paris-Saclay, Université de Versailles Saint-Quentin-en-Yvelines (UVSQ), Sorbonne Université, Centre National de la Recherche Scientifique (CNRS), Guyancourt, France
[6] Applied Physics Laboratory, Johns Hopkins University, Laurel, MD, USA
Received 2024 March 7; revised 2025 July 29; accepted 2025 July 29; published 2025 September 16

Abstract

Understanding the lake–atmosphere interactions on Titan is crucial to answering some of Titan's long-standing scientific questions, such as the unexpectedly high methane abundance close to the surface, or the "magic islands" that appear on one of the seas. Here we focus on specific lakes called Sharp-Edged Depressions, which are surrounded by high-elevation terrains called ramparts with unique structural and spectral properties. We aim at understanding how topography and surface properties around the lakes affect air–surface interactions. To study the effect of ramparts, we utilize the mtWRF model configured in 2D. We model a variety of lake morphologies: those surrounded by hills (300 m high, 30 km wide), those with no surrounding topography, and those at the bottom of a depression. To encapsulate the effects of surface properties, we vary the surface roughness, albedo, and thermal inertia. We also consider the effect of varying the background wind and the season. Our model indicates that the addition of topography creates weaker winds over the lake ($\approx -30\%$) and reduces the quantity of methane evaporated ($\approx -10\%$) compared to the no-topography case. However, topography results in deeper vertical transport of methane and deepens the marine layer (from a few meters to ≈ 50 m). Higher roughness (from 0.4 to 40 cm) of the ramparts tends to decrease the wind speed ($\approx -50\%$) and reduces the horizontal extension of the lake breeze ($\approx -20\%$). Albedo and thermal inertia variations have a negligible effect. Seasons have a strong effect on the evaporation of methane, with evaporation rates nearly 3 times higher in summer than in winter.

Unified Astronomy Thesaurus concepts: Titan (2186); Atmospheric dynamics (2300); Planetary atmospheres (1244); Surface processes (2116); Ocean-atmosphere interactions (1150); Land-atmosphere interactions (900)

1. Introduction

Titan, the largest moon of Saturn, is the only moon of the solar system to have a substantial atmosphere, with a surface pressure of 1.5 bar. Its atmosphere is composed primarily of nitrogen (95%) and methane (5%), with trace amounts of higher-order hydrocarbons and nitriles. The high concentration of methane is surprising, since this component is destroyed in the upper atmosphere by photodissociation. Without a resupply mechanism, the atmosphere would be depleted of methane in 10^7–10^8 yr (A. G. Hayes et al. 2018). To understand the evolution of methane on Titan over geological timescales, one key ingredient is a better assessment of short-term surface–atmosphere exchanges. One of the main expected sources of atmospheric methane on Titan is the evaporation from hydrocarbon lakes; however, their evaporation rate is not well constrained. Prior model estimates predict evaporation rates ranging from 0.2 to 10 m yr^{-1} (G. Mitri et al. 2007; A. Chatain et al. 2022). More detailed modeling of the interactions between the lakes and the atmosphere may further constrain this range, as well as help understand the more general methane cycle, including the formation of clouds. Modeling can also test some formation hypotheses of "magic islands" formation, which are bright surfaces appearing in radar images. They indicate a transient rough surface of the sea, possibly due to increased wind speed (J. D. Hofgartner et al. 2016), among other mechanisms (e.g., X. Yu et al. 2024).

Lakes morphologies on Titan can be divided into two main categories: (1) broad, open basins associated with river networks and (2) smaller, rounder depressions, surrounded by steep borders (A. Hayes et al. 2008; A. G. Hayes 2016; S. Birch et al. 2018). The latter are called Sharp-Edged Depressions (SEDs). Approximately 75% of the SEDs are surrounded by topography structures (S. P. D. Birch et al. 2019) a few hundred meters high and a few kilometers wide (E. R. Stofan et al. 2007; R. J. Michaelides et al. 2016; S. P. D. Birch et al. 2019; G. Mitri et al. 2019). We will later refer to these high-elevation features surrounding some SED lakes as "ramparts," following A. Solomonidou et al. (2019). Some of these ramparts appear bright in radar data (C. A. Wood et al. 2006; S. P. D. Birch et al. 2019; G. Mitri et al. 2019) suggesting surface properties that differ from the surrounding plains. While the formation mechanism of these ramparts is undetermined, current hypotheses include volcanic calderas (C. A. Wood et al. 2006), impact craters (A. G. Hayes et al. 2017), sublimation-erosion mechanisms (S. P. D. Birch et al. 2019), karst-hardened postdeflation remnants (A. Solomonidou et al. 2019), or vapor explosions close to the surface (G. Mitri et al. 2019; G. E. Brouwer et al. 2024).

Here, we will focus on the effect of the SED lakes and their associated ramparts on the local atmospheric circulation. We run mesoscale atmospheric simulations (typically 100s km domains

Table 1
Typical Surface Properties Used for Some Titan Terrains

	Thermal Inertia I ($J\,m^{-2}\,K^{-1}\,s^{-0.5}$)	Surface Roughness[b] z_0 (cm)	Albedo[c] α
Plains	601[a]	0.4	0.3
Labyrinths	808[a]	40	...
Lakes	Not Applicable (1 m mixing layer in our model)	0.01	0.1
Land values used in this work	601	0.4	0.3
Ramparts values used in this work	808	40	0.4

Notes. The values considered plausible for some Titan terrains (plains, labyrinths, and lakes) are compared to the values used in this work.
[a] Values from S. M. MacKenzie et al. (2019b).
[b] Surface roughness values are estimated, using C. Baciocco (2021) as a guideline. See Section 3.3.1.
[c] See Section 3.3.2 for a discussion on chosen albedo values.

with 1–10 km grid size) using the mesoscale Titan Weather Research and Forecasting (mtWRF) model (S. C. R. Rafkin & A. Soto 2020, described in Section 2). Previous works with this model have shown that lakes on Titan create lake breeze circulations (S. C. R. Rafkin & A. Soto 2020), varying throughout the day (A. Chatain et al. 2022) and depending on the lake shape (A. Chatain et al. 2024). We aim to quantify the impact of lake ramparts on the lake breeze and on the lake–atmosphere interactions. We run the model in 2D (i.e., with a vertical axis and only one horizontal axis), and in idealized mode (i.e., with simplified initialization fields, due to the scarcity of the data available at this scale on Titan). We study the effect of adding a simple topography and the effect of having different surface properties at the ramparts (surface roughness, albedo, and thermal inertia). Finally, we investigate the effect of adding background winds and of changing the season.

Several lines of evidence suggest that the ramparts have surface properties that differ from the surrounding land. The brightness of the ramparts in radar images suggests a high surface roughness (C. A. Wood & J. Radebaugh 2020). A. Solomonidou et al. (2020) also showed that ramparts have a different spectral signature from the surrounding terrains and that they seem to be similar to the labyrinth terrains. In addition, S. M. MacKenzie et al. (2019b) estimated thermal inertia values for the different terrains on Titan based on expected chemical compositions and physical properties. In their model, the thermal inertia of the labyrinth terrains is higher than the thermal inertia of the plains (Table 1).

The model simulation configurations are described in Section 2. The results are presented in Section 3. We first present the reference case (Section 3.1). Then, we move to the effects of topography and seasons (Section 3.2) and surface properties (Section 3.3). Finally, we present our main conclusions and some perspectives in Section 4.

2. Model Description (mtWRF)

2.1. Global Description and Schemes

We use the mtWRF model (S. C. R. Rafkin & A. Soto 2020), with additional updates to the schemes corresponding to radiative transfer, surface and subsurface temperatures, and turbulence (A. Chatain et al. 2022, 2024). The mtWRF model is based on the Weather Research and Forecasting (WRF) model (C. Skamarock et al. 2008) developed at the National Center for Atmospheric Research. The model was developed for Titan from WRF by S. C. R. Rafkin & A. Soto (2020) and used to model the atmospheric circulation around a methane lake. A. Chatain et al. (2022) then added a radiative transfer scheme to the model. In this study, we focus on the influence of surface properties and topography around the lake using idealized 2D simulations.

We use a simple thermal diffusion scheme, modified from A. K. Blackadar (1979) and J. Dudhia (1996), to model the interaction between the subsurface and the surface. The surface layer is modeled by an Eta similarity scheme, implemented by A. S. Monin & A. M. Obukhov (1954), Z. I. Janjić (1994), Z. I. Janjić (1996), and Z. I. Janjić (2001). The sensible and latent heat fluxes are computed through a turbulence closure model described in Z. I. Janjić (2001), and the saturation vapor pressure is computed for pure methane following J. I. Moses et al. (1992). More details on the turbulence scheme used in our model are presented in A. Chatain et al. (2024; Appendix 1). The planetary boundary layer (PBL, the layer in which winds are influenced by surface friction) is modeled by the Mellor–Yamada–Janjic scheme (F. Mesinger 1993; Z. I. Janjić 1994). A. Chatain et al. (2022) described the radiative transfer scheme, the slab lake model, and the methane exchanges between the lake surface and the atmosphere. In this work, we do not model methane exchanges between the land and the atmosphere (which is not trivial and planned for future studies).

In A. Chatain et al. (2022), the emissivity was set to 0.9 all over the domain. The comparison between teledetection temperature retrievals using Cassini/CIRS and the in situ temperature measurements with Huygens/HASI suggests a surface emissivity close to unity (D. E. Jennings et al. 2011). Here we use an emissivity of 0.95 for the land, a value taken from the results obtained in R. M. C. Lopes et al. (2016) from the Cassini Radar data for undifferentiated plains. For the lake, we take an emissivity of 0.99 (A. Le Gall et al. 2016, in the microwave range). The lake breeze shape remains similar to results obtained with an emissivity set to 0.9 (see Appendix A).

2.2. Model Initialization and Configuration

In this work, the latitude is set to 74°N, consistent with the general location of the SED lakes. For the initialization of the pressure, air temperature, and methane mixing ratio, we use values from the Titan Atmospheric Model (TAM, a general

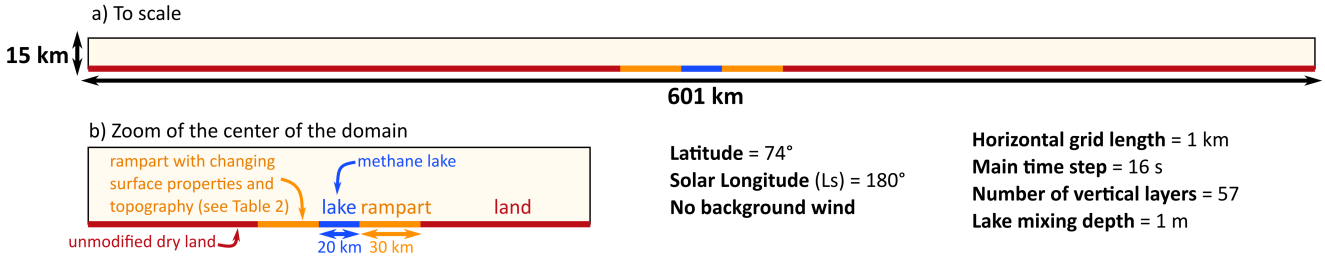

Figure 1. Diagram of the model domain. (a) To scale. (b) Magnification of the center of the domain. Bottom right: values for some important parameters, left constant for this study. Remark: 16 s corresponds to 1 Titan second.

circulation model described in J. M. Lora et al. 2015; and J. M. Lora et al. 2022) at 74°N at autumn equinox, over a lake. To facilitate interpretation of the simulated processes, we use a zero wind background state (the effect of background wind is discussed in Section 3.2.3).

The simulation domain has a vertical top at 15 km, with a damping layer of 5 km at the top. The domain is 600 km wide, large enough to avoid numerical resonances at the boundaries. The model is divided into 57 vertical layers. The horizontal resolution is 1 km. The center of the domain is occupied by a pure methane lake surrounded by dry land (Figure 1). The lake is 20 km in diameter, a typical size for a SED. In our simulations, we modified the surface properties and the topography of the land within 30 km from the lake shores (we call these 30 km "ramparts"). The model needs a few Titan days (tsols; 1 tsol is 15.95 Earth days) to spin-up a diurnally repeatable circulation (typically 2 to 4 tsols). Thus, we analyzed the 5th and 6th days of simulation.

We used an idealized topography, smoothed to avoid numerical instabilities. The shape of the topography was adapted from a mathematical function called *smootherstep*, defined as $y = 6x^5 - 15x^4 + 10x^3$. We compute this function from $x = 0$ at the lakeshore (i.e., 10 km from the lake center) to $x = 1$ at the rampart's top (i.e., 25 km from the lake center). It is then multiplied by the maximum height of the rampart (i.e., 300 m in this study). The rest of the rampart, from the top to the land, is completed by symmetry. This smooth topography enables the model to minimize errors associated with the calculation of horizontal gradients from the terrain-following coordinate system.

The lake exchanges methane with the atmosphere through evaporation. Only the lake evaporates methane; the land is considered to be in equilibrium with the atmosphere. Condensation is not allowed, neither at the surface nor in the atmosphere. In the simulations performed for this work we do not reach saturation conditions; thus, we would not expect condensation even if a microphysics scheme was implemented.

Some important constants in this study are listed on Figure 1.

Figure 2 is a list of all the simulations that will be discussed thereafter, except for the background wind and season runs. To study the effect of the background wind, we made two additional runs with background wind, one with topography similar to the reference simulation, and one with flat topography. For the seasons, four additional runs were launched, similar to the reference run for everything except for the background wind and for the insolation. They correspond respectively to the autumn equinox, winter solstice, spring equinox, and summer solstice. The background wind used comes from outputs of the TAM model at 74°N; see Figure 3.

3. Results

In this section, we show some results for the simulations described in Figure 2. For more quantitative values of latent heat flux and winds, the reader is referred to tables in doi:10.5281/zenodo.14833640.

3.1. Reference Simulation

In the reference simulation (Simulation R; see Figure 2) the methane lake is surrounded on each side by hills of 300 m in elevation and 30 km in horizontal width. Methane evaporates from the lake to the subsaturated atmosphere immediately upon model integration. The average latent heat flux over the lake after spin-up is 0.39 W m^{-2}.

The lake cools through the latent heat flux (see Figure 4(a)), and the equilibrium lake surface temperature is lower than the land surface temperature, as shown in Figure 4(b). Sensible heat flux with the atmosphere results in colder air above the lake (from 91.1 to 91.3 K) than above the ramparts (from 91.5 to 92 K). This temperature gradient drives a thermally direct lake breeze circulation, with air flowing from the lake to the land close to the surface and from the land to the lake at the top of the mixed layer.

As found in a previous work performed with mtWRF (A. Chatain et al. 2022), the lake breeze varies diurnally: the lake breeze front is close to the shoreline during the day and moves inland during the night (see Figures 4(c), (d) and 5). The diurnal behavior is due to turbulence, which diffuses the different air masses at the lake breeze front more strongly during the day. Indeed, the turbulent kinetic energy (TKE) is larger during the day, due to solar heating of the surface driving larger sensible heat fluxes to the atmosphere (see Figure 4(e)).

Figure 5 shows the horizontal and vertical winds at 2 a.m. and 2 p.m.. Close to the surface, we can see the circulation going from the cold lake to the warmer land, and higher in altitude, we see the return branch going from the land to the lake. Above the lake, the maximum horizontal wind is around 0.04 m s^{-1} at the surface (i.e., in the first vertical layer). Over the full domain, the maximum horizontal wind at the surface is 0.2 m s^{-1}, reached at the ramparts with the dense cold air from above the lake flowing downhill (katabatic winds). The average horizontal wind is 0.013 m s^{-1} above the lake and 0.070 m s^{-1} above the ramparts.

Simulation	Topography shape	Lake or no lake?	**Surface properties of the rampart**			Description
			$z0$ [cm]	α [%]	I [J m^{-2} K^{-1} s$^{-0.5}$]	
R "Reference"		lake	0.4	30	601	Reference simulation
F "Flat"		lake	0.4	30	601	Flat topography
D "Dry"		no lake	0.4	30	601	Land everywhere (Dried lake)
H "Hole-shaped"		lake	0.4	30	601	Hole-shaped topography
Z "Z0"		lake	**40**	30	601	Higher surface roughness (z0)
A "Albedo"		lake	0.4	**40**	601	Higher albedo (α)
I "Inertia"		lake	0.4	30	**808**	Higher thermal inertia

Figure 2. List of the simulations used in this work. z0: roughness length, α: albedo, and I thermal inertia. Bold highlights the parameters changes compared to the reference simulation. The topography shape is described in more detail in Section 2.2, and the terrain relief is 300 m in each case.

The expected change in lake level associated with evaporation may be calculated as $\Delta h = \frac{\mathrm{LH}}{\rho \times L_v}$, with LH the latent heat flux to the surface. At Titan's surface temperature and pressure, the liquid methane has a density $\rho \approx 447\,\mathrm{kg\,m^{-3}}$ and a latent heat of vaporization $L_v \approx 5.1 \times 10^5\,\mathrm{J\,kg^{-1}}$. We obtain a level change of approximately $-5.4\,\mathrm{cm\,yr^{-1}}$ (with yr indicating one Earth year). Locally, a higher value is obtained at the lake borders ($\approx -6.1\,\mathrm{cm\,yr^{-1}}$), and a lower value is calculated at the lake center ($\approx -5.2\,\mathrm{cm\,yr^{-1}}$). We also observe diurnal changes: there is more evaporation during the afternoon (LH$\approx -0.42\,\mathrm{W\,m^{-2}}$) than during the morning and night (LH $\approx -0.35\,\mathrm{W\,m^{-2}}$), as can be seen on Figure 4(a).

3.2. Impact of Topography on Mesoscale Atmospheric Dynamics

3.2.1. Effect of Topography without the Lake: Slope Winds

In this section, we investigate the effect of topography alone on the local winds, without the lake. Two 300 m hills separated by 20 km are considered (see simulation D in Figure 2).

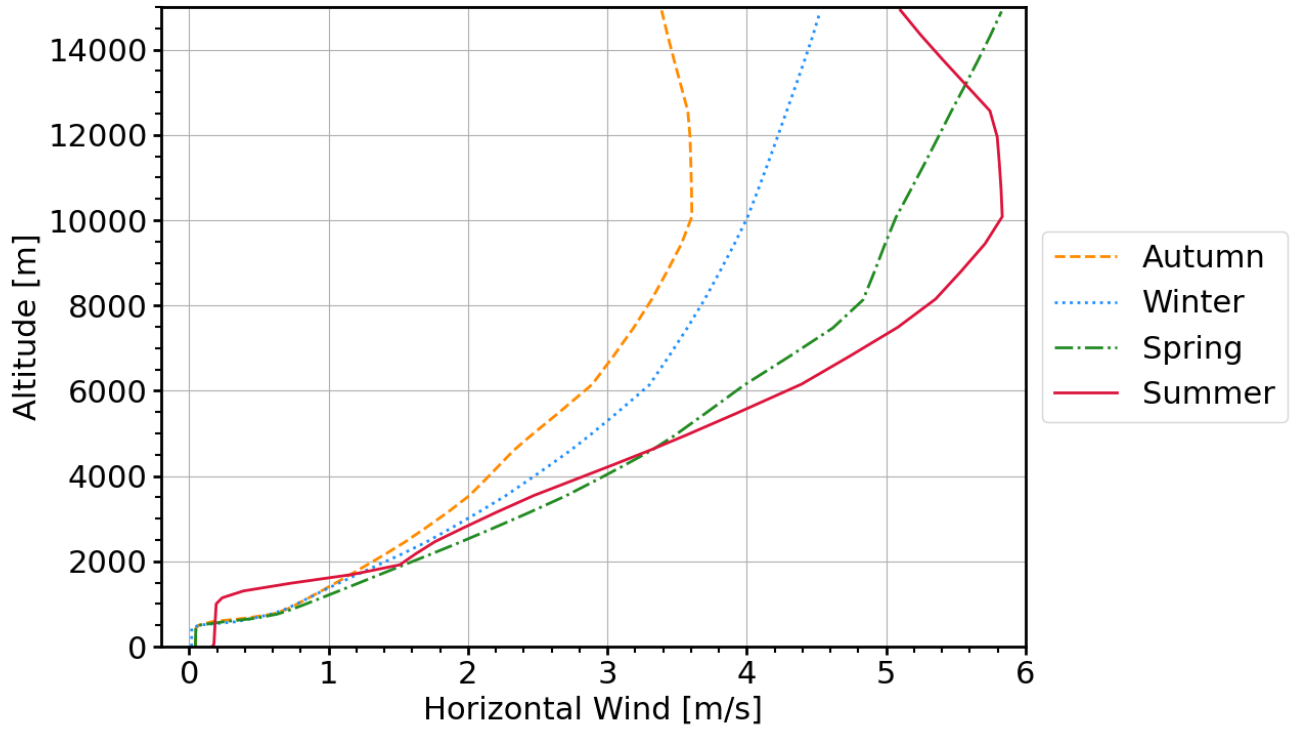

Figure 3. Horizontal background wind used for the season runs (from the TAM model at 74°N; J. M. Lora et al. 2022). For the background wind runs, the autumn profile is used.

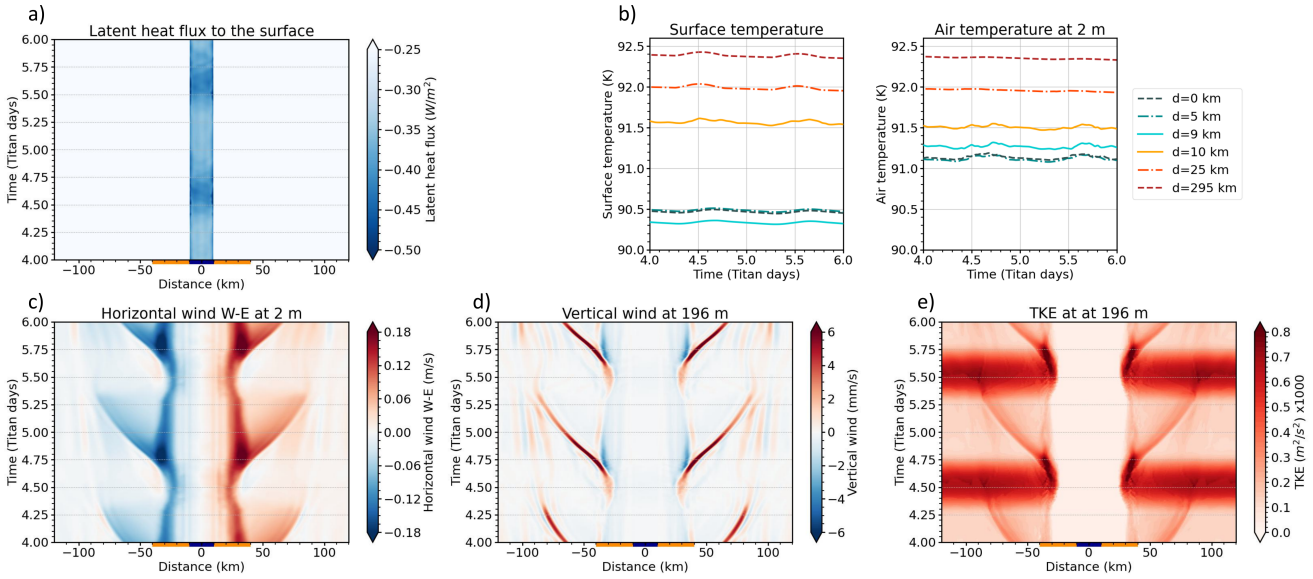

Figure 4. Reference simulation: evolution with time of the (a) latent heat flux to the surface and (b) surface temperature and air temperature at different locations (0, 5, and 9 km: above the lake; 10, 25, and 295 km: above land). (c) Horizontal wind at 2 m above the surface, i.e. the first horizontal level of the model (positive values indicate wind blowing to the right), (d) vertical wind at ≈200 m above the surface (positive values indicate upward wind), and (e) turbulent kinetic energy (TKE) at ≈200 m above the surface. The time axes start at the end of the 4th tsol, at midnight. The blue bar at the bottom of the plots shows the location of the lake. The orange bars show the location of the ramparts.

This configuration produces upslope winds (Figure 6). The maximum horizontal wind close to the surface is around 10 cm s^{-1}, and the maximum vertical wind is around 5 mm s^{-1}. At the top of each hill, convergence of the horizontal wind and thermal buoyancy generate an updraft. Compensating subsidence is found above the crater. The upslope winds are present day and night (see Figures 6(c) and (d)). The intensity of the observed updraft is higher between 2 p.m. and 8 p.m., when the daytime solar insolation increases the buoyancy of the surface air through sensible heat flux (the updraft wind speed reaches ≈5 mm s^{-1}). In contrast, Earth, Mars, and Venus usually generate downslope nighttime slope winds in addition to the daytime upslope winds (H. Savijärvi & T. Siili 1993; S. Lebonnois et al. 2018; B. J. Hatchett et al. 2020; S. Farina & D. Zardi 2023). The unique solution on Titan is due to a higher net infrared flux into the surface at the

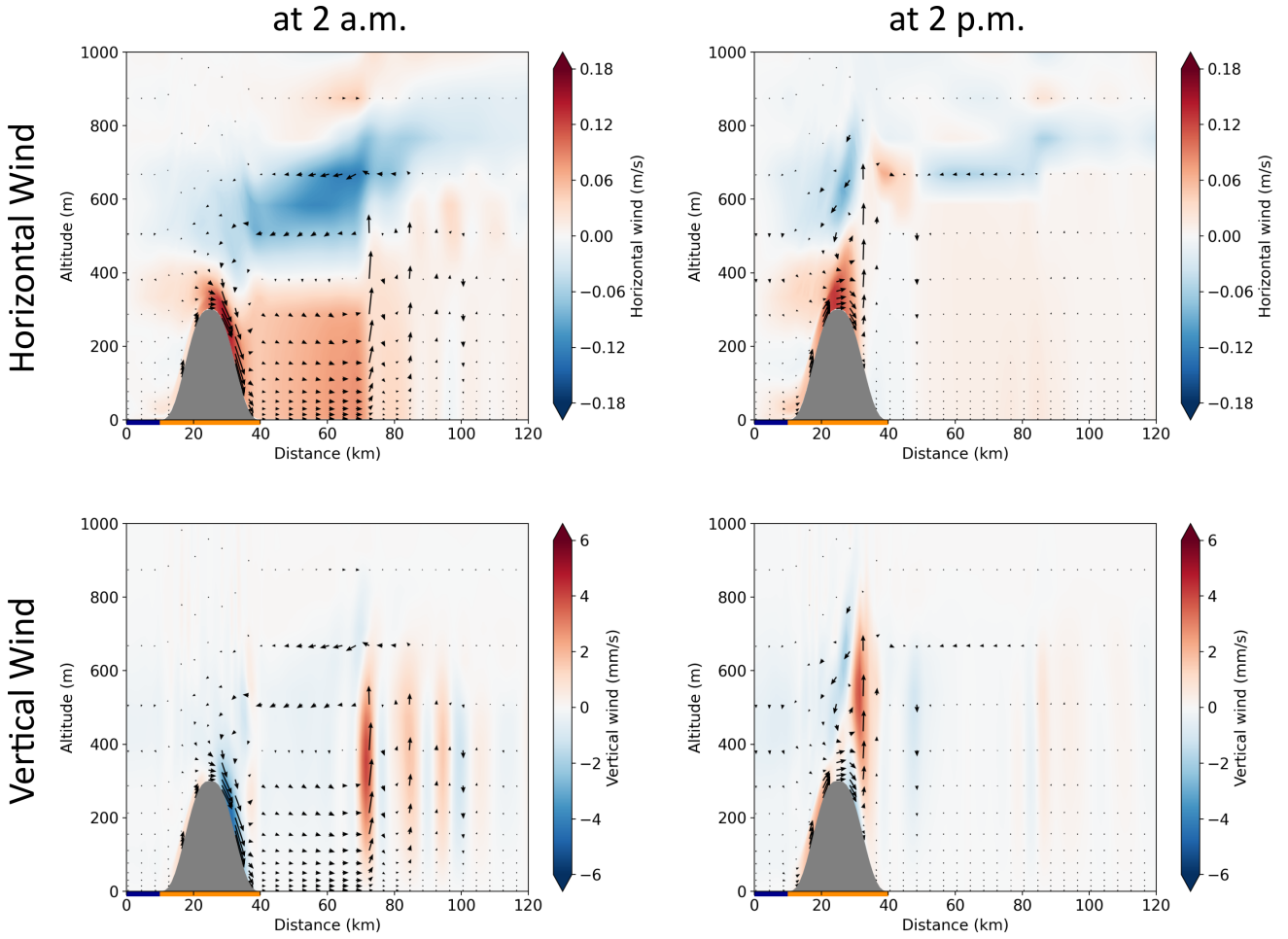

Figure 5. Wind circulation in the reference simulation. Left column: at 2 a.m. Right column: at 2 p.m.. Top row: horizontal wind. Bottom row: vertical wind. The blue bar under the plots shows the position of the lake. The orange bar corresponds to the rampart position.

top of the topography than at the bottom: as shown in Figure 7, the net infrared flux to the surface is approximately 3 times larger ($+0.013\,\mathrm{W\,m^{-2}}$) at the top of the hill (25 km from the domain center) than at the bottom (10 km from the domain center). As a result, the sensible heat flux to the atmosphere is higher at the top of the topography than at the bottom, which results in a temperature inversion. During the day, the solar flux warms the surface and enhances the phenomenon, resulting in more intense upslope winds at the end of the afternoon (see Figure 6). Thus, the simulation predicts only upslope winds in dry craters at this season (autumnal equinox). At other seasons or other latitudes (in this work we are at 74° N), slope winds could be different on Titan.

If a lake is added in the crater between the hills, the upslope winds are overwhelmed by the lake breeze (see Section 3.1).

3.2.2. *Effect of the Shape of the Ramparts*

In this section, we examine the effect of the shape of the ramparts on the local lake breeze. Three shapes are considered (see Figure 8, which shows the right part of the domain; the other part is symmetric): (1) a flat topography (Simulation F), (2) a lake surrounded by two hills (Simulation R), and (3) a lake in a topographic low, surrounded by higher-elevation land (Simulation H, referred to as "lake in a depression").

With hill-shaped ramparts, the lake breeze penetrates less over land ($\approx -20\%$) compared to the flat-topography environment (see Figure 8). For the lake in a depression, the breeze penetrates farther over land than in the flat-topography case ($\approx +5\%$). The maximum surface wind is around $0.15\,\mathrm{m\,s^{-1}}$ for the flat topography and the lake in a depression, while it is slightly more intense in the reference case, around $0.2\,\mathrm{m\,s^{-1}}$. This is probably due to the gravitational acceleration downward along slopes of the cold air coming from the lake. However, on average, the surface horizontal wind is 50% weaker in the reference case than in the flat and depression cases (the higher maximum wind does not compensate for the overall fainter wind). The horizontal wind over the full depth of the PBL exhibits the same general trends as the surface wind. Above the lake, the maximum surface wind is around $0.06\,\mathrm{m\,s^{-1}}$ in the flat-topography case, while it is 30% weaker for the simulations with topography (the maximum speed at the surface is around $0.04\,\mathrm{m\,s^{-1}}$ for both the lake in a depression and the hills) because more energy is needed for the dense air above the lake to go over the topography.

The methane is advected to higher altitudes in cases with topography (see Figure 8, bottom row), forming a deeper marine layer. The marine layer is the cold, stable layer formed above the lake or close to the lake. In Figure 8, the marine layer is visually identified by the high methane mixing ratio (dark blue colors). In the flat case, the methane marine layer is confined to the first vertical layer of the model, i.e., within a few meters above the lake, while the marine layer is 50 m deep with the

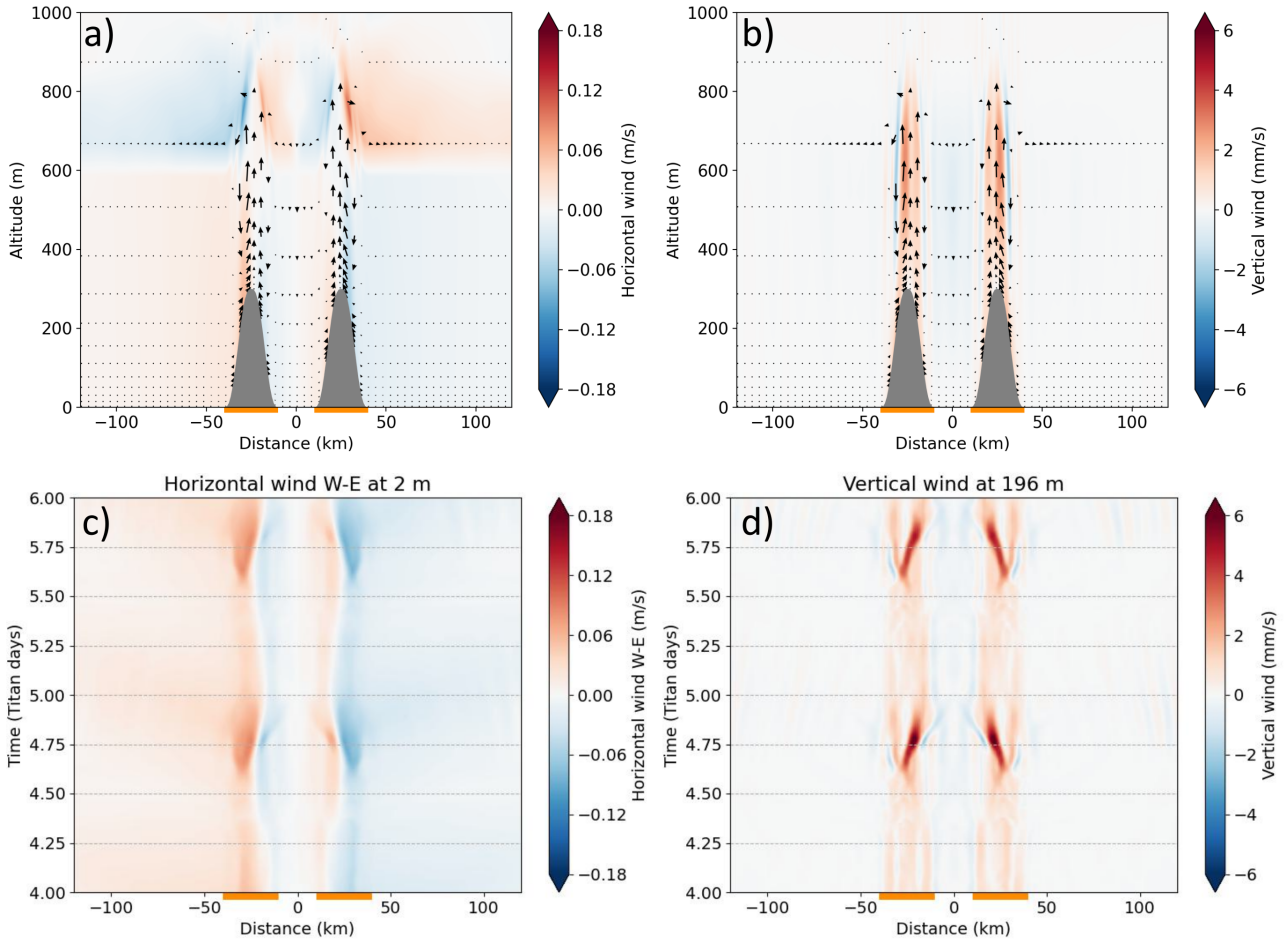

Figure 6. Dry simulation. Left column: horizontal wind. Right column: vertical wind. Top row: circulation at 2 p.m. Bottom row: evolution of horizontal wind at 2 m above the surface (c) and evolution of vertical wind at 200 m above the surface (d). The orange bars below the plots show the ramparts' location.

addition of topography. The surface methane mixing ratio is similar in the three simulations, around 43 g kg^{-1}. The overall distribution of methane in the atmosphere also changes, due to the effect of topography on the atmospheric circulation, which transports the methane evaporated to the atmosphere. In the flat case, the upward motion along the lake breeze front injects methane up to 700 m into the atmosphere. When hills are added, the methane injected reaches nearly 1000 m. Less methane is evaporated overall when topography is added; we obtain an evaporation rate of ≈6 cm yr^{-1} in the flat environment, while with topography, it is approximately 10% lower (≈5.5 m yr^{-1}).

Finally, in our simulations, the relative humidity of methane never reaches 100%, and thus, no methane condensation is expected (the maximum relative humidity values are between 84% and 88%). However, fog has possibly been observed on Titan at the latitudes of the northern lakes (M. E. Brown et al. 2009b), which means that methane condensation may occur near the surface. More work is needed to assess the effect of turbulence parameterization, season, and time of the day, among other parameters, on the relative humidity around Titan lakes, but this is beyond the scope of this paper. Our study suggests that among the three topographies considered (flat, ramparts, and lake in a depression), the rampart shape causes the highest maximum relative humidity, while in the flat shape case, lower relative humidities are reached.

Appendix B shows a case with two lakes and ramparts. In this situation, the two lake breezes merge, and methane accumulates between the lakes, which increases the relative humidity above the central rampart.

3.2.3. Effect of Background Wind and Seasons

In this section, we consider the effect of adding background wind to the simulations. We then make the background wind and the insolation vary to study the effect of the different seasons.

In our simulations, the effect of adding background wind is faint. In particular, it does not change strongly the evaporation since the lake breeze prevents the appearance of strong winds above the lake. In 3D, adding background wind has been shown to have a significant impact on the lake breeze (A. Chatain et al. 2024). In our simulations we find similar behaviors for the lake breeze, but in our case, the lake evaporation is nearly unchanged, due to the small size of the lake we study and the presence of topography that protects the lake. Also, some effects described in A. Chatain et al. (2024), such as the formation of an accelerated wind pocket behind the lake, are not observed here due to the 2D geometry.

On the contrary, the seasons influence strongly the evaporation rate, which is at minimum during winter (≈4.5 cm yr^{-1}) and at maximum during summer (≈ 13 cm yr^{-1}). The seasons also influence the PBL depth, which goes from 300 m in winter to around 1200 m in the summer. Figure 9 represents the horizontal wind for each season. It shows that the turbulent layer

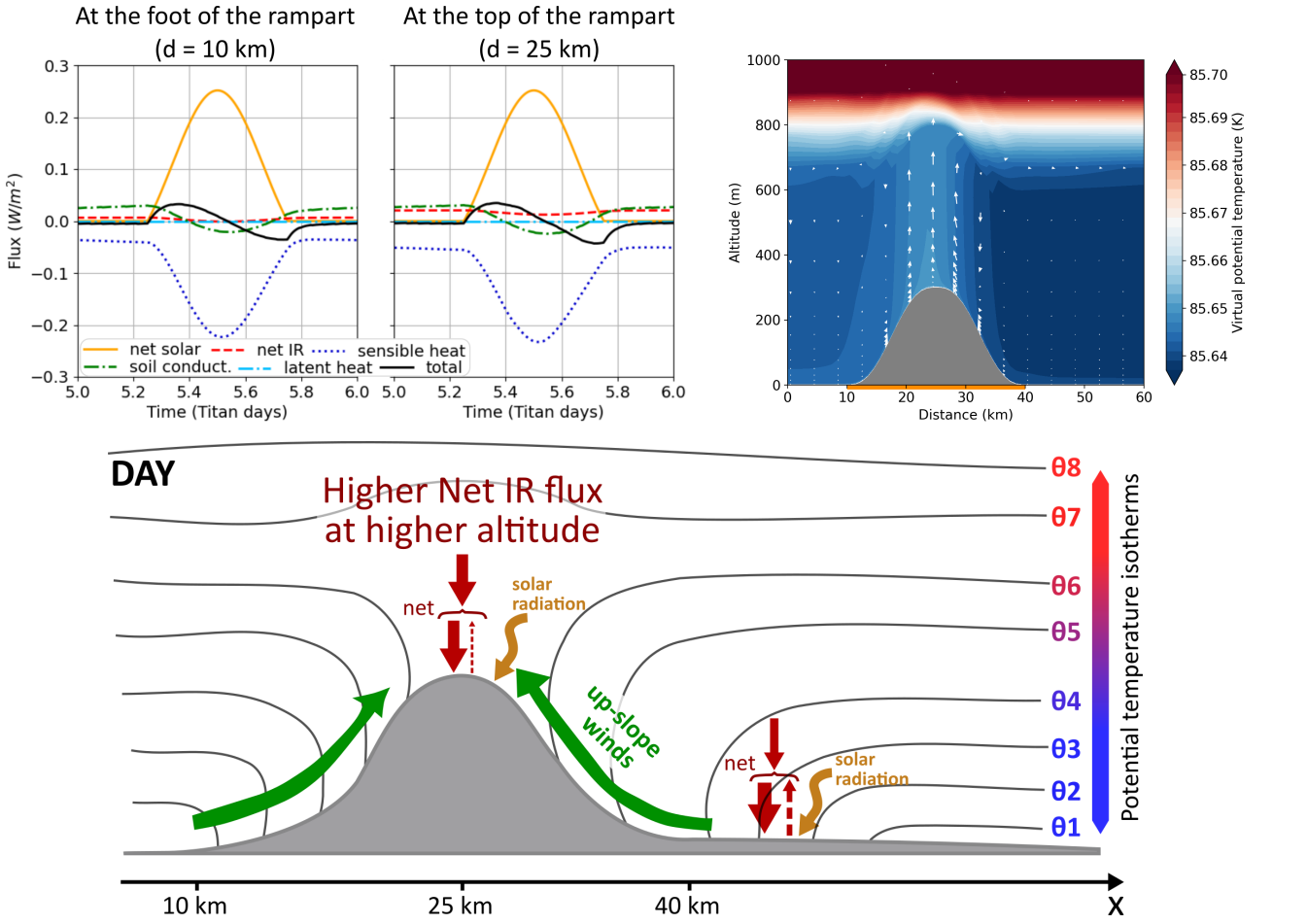

Figure 7. Top left: fluxes to the surface, in W m^{-2}, at 10 km from the center of the domain (i.e., at the foot of the rampart) and at 25 km from the center of the domain (i.e., at the top of the rampart.). Top right: virtual potential temperature at 2 p.m. Bottom: mechanisms explaining the upslope winds on Titan. The gradient of potential temperature on the slopes is created by the difference of infrared flux emitted by the surface, which is colder in altitude and thus emits less infrared. Note the negative vertical gradient in potential temperature at the rampart surface. We observe upslope winds 24 hr a day.

is deeper in summer and that for all seasons except summer, the lake is protected from the wind by the lake breeze, which can explain the higher evaporation rate in the summer.

3.3. Impact of Surface Properties on Mesoscale Atmospheric Dynamics

In this section, we focus on the effect of surface roughness, albedo, and thermal inertia. The details are presented below. In a nutshell, increasing the roughness from 0.4 to 40 cm has a noticeable impact on the winds, on the lake evaporation, and on the surface and air temperatures. However, it does not change the global shape of the lake breeze. Changing the albedo from 0.3 to 0.4 and the thermal inertia from 601 to 808 J m^{-2} K^{-1} $s^{-0.5}$ has a negligible effect.

3.3.1. Surface Roughness

In this section, we focus on the effect of increasing the surface roughness of the ramparts, from 0.4 to 40 cm (Simulation Z). The surface roughness, also called surface roughness length, is an empirical parameter corresponding to the altitude above the surface at which the horizontal wind is null in the logarithmic velocity profile equation of the horizontal wind (P. S. Arya 2001). The surface roughness length is proportional to the mean height of the roughness elements and their density (H. Lettau 1969; J. R. Garratt 1977).

Some rampart features appear bright in Cassini Radar images (S. P. D. Birch et al. 2017; G. Mitri et al. 2019; A. Solomonidou et al. 2020; C. A. Wood & J. Radebaugh 2020), which suggest a higher surface roughness than the surrounding plains (less bright). C. Baciocco (2021) estimated the order of magnitude of surface roughness for several Titan terrain types, based on Earth analogs. Lake ramparts are spectrally similar to labyrinthic terrains (A. Solomonidou et al. 2020). Thus, we decided to use a roughness close to the labyrinth's roughness. In C. Baciocco (2021), the plains are associated with a roughness of the order of 1×10^{-3} m and the labyrinth terrains with a roughness of the order of 1 m. For comparison, T. Tokano et al. (2006) estimated the surface roughness at the Huygens landing site around 5×10^{-3} m, while R. D. Lorenz (2021) estimated 1×10^{-4} m for the roughness of "an extremely flat surface." In this study, we estimated that plains surrounding lakes at the north pole were a little rougher than Titan tropical plains due to the probable presence of many small rain drains around the lakes. Indeed, precipitation is expected to be more intense and common at high latitudes compared to the tropics (S. P. Faulk et al. 2017). We also estimated that ramparts were probably a little less rough than large structures of labyrinthic terrains. Therefore, in this simulation, we used a roughness of

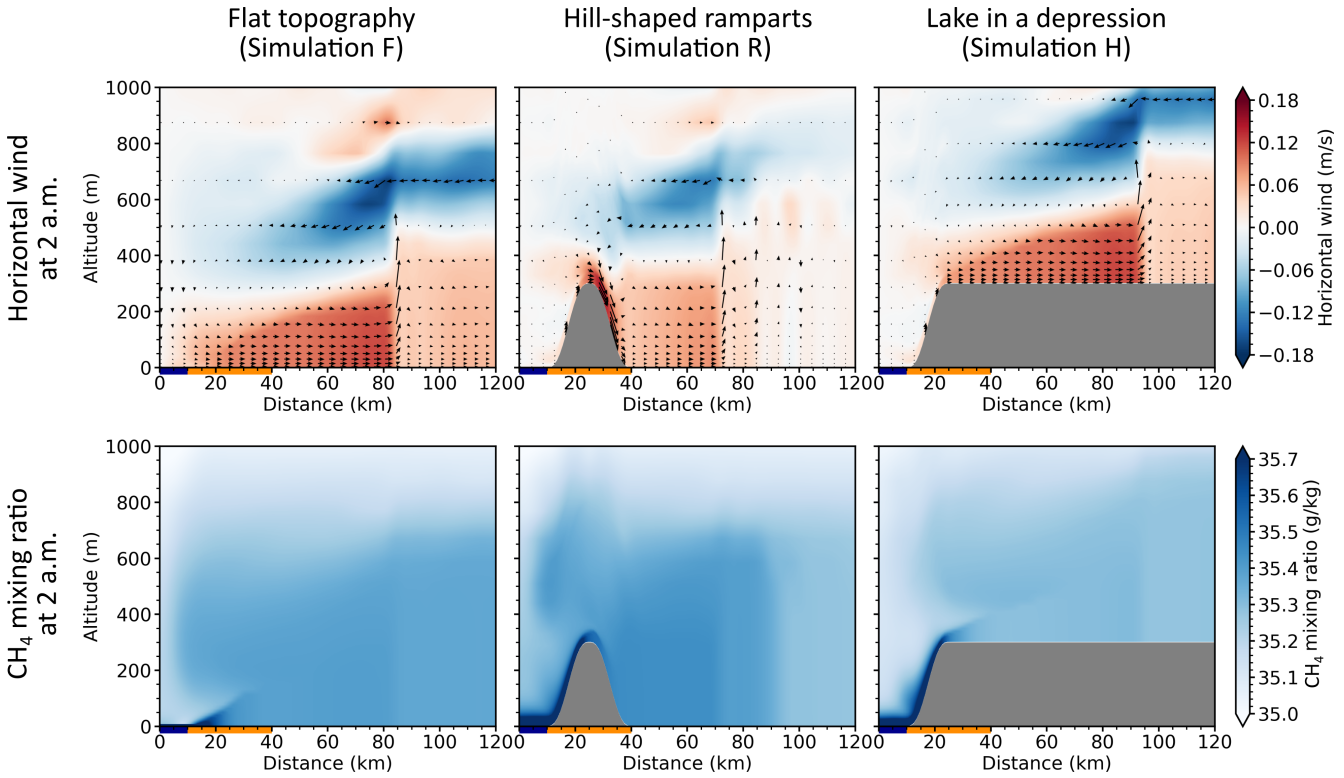

Figure 8. Comparison of different topographic shapes for the ramparts. Left column: flat topography. Middle column: hill-shaped ramparts (reference run, simulation R). Right column: lake in a depression. Top row shows the horizontal wind at 2 a.m. Bottom row shows the CH_4 mixing ratio at 2 a.m. Note the position of the lake breeze front around 75 km for the hill-shaped ramparts, 85 km for the flat topography, and 95 km for the lake in a depression, materialized by a steep change in horizontal wind and methane mixing ratio.

4×10^{-4} m for the plains and of 4×10^{-1} m for the ramparts. In the previous simulations, the surface roughness was set to 4×10^{-3} m everywhere on land.

Results are presented in column 2 of Figure 10. We observe that the global shape of the lake breeze is unmodified. However, close to the surface, the horizontal wind is strongly slowed above the ramparts ($\approx -50\%$). Moreover, the mixing near the surface is increased (see the TKE panels). The latent heat flux over the lake varies throughout the day compared to the reference simulation: there is less evaporation in the early afternoon, because the wind is slowed down by the roughness (see the "horizontal wind at 2 m" panels). At the lake border, we observe the opposite: the evaporation is higher, due to a higher turbulence. The surface temperature of the lake is slightly warmer, because there is less evaporation at the lake center. The surface temperature at the ramparts is slightly colder, probably linked to the higher turbulence there.

3.3.2. Albedo

In this section, we consider the effect of increasing the surface albedo of the ramparts, from 0.3 to 0.4 (Simulation A). Some Cassini data show evidence for brighter ramparts than the surrounding terrains in visible and infrared light (Cassini VIMS; see S. M. MacKenzie et al. 2019a, their Figure 1.), suggesting a higher surface albedo. However, the albedo depends on wavelength, while in our model the albedo refers to a global albedo for short wavelengths (i.e., mainly the visible range). Moreover, the data do not show unambiguously that the ramparts' albedo is higher. For instance, in the infrared domain, the ramparts seem to have a lower albedo than the surrounding land (A. Solomonidou et al. 2020). Thus, this simulation aims only to assess what would be the effect of a different albedo terrain around the lakes, not to give a realistic albedo value for the ramparts.

In the reference simulation, the albedo was set to 30% for the land and 10% for the lake. In Simulation A, we set the albedo of the rampart to 40%. As expected, we observe a lower net shortwave flux absorbed by the surface of the ramparts (by definition). However, there is only a small effect on the surface temperature (on average -5×10^{-3} K over the ramparts). The structure of the lake breeze remains unchanged.

3.3.3. Thermal Inertia

In this section, we consider the effect of increasing the ramparts' thermal inertia, from 601 to 808 $\mathrm{J\,m^{-2}\,K^{-1}\,s^{-0.5}}$ (Simulation I). A. Solomonidou et al. (2020) showed that the spectral properties of the ramparts are close to the labyrinth terrain properties, and these terrains have a thermal inertia approximately 30% higher than the plains' thermal inertia (S. M. MacKenzie et al. 2019b, see Table 1). Knowing that thermal inertia has an influence on the heat transfers between the surface and the atmosphere, it is an important property to investigate.

In the reference simulation, the land thermal inertia was set to 601 $\mathrm{J\,m^{-2}\,K^{-1}\,s^{-0.5}}$, the value assigned to plains in S. M. MacKenzie et al. (2019b). In Simulation I, the ramparts' thermal inertia was set to 808 $\mathrm{J\,m^{-2}\,K^{-1}\,s^{-0.5}}$, the value assigned to labyrinths in S. M. MacKenzie et al. (2019b). Figure 10 shows that such a change has only a very small effect on the lake breeze. It can thus be neglected compared to the effect of roughness.

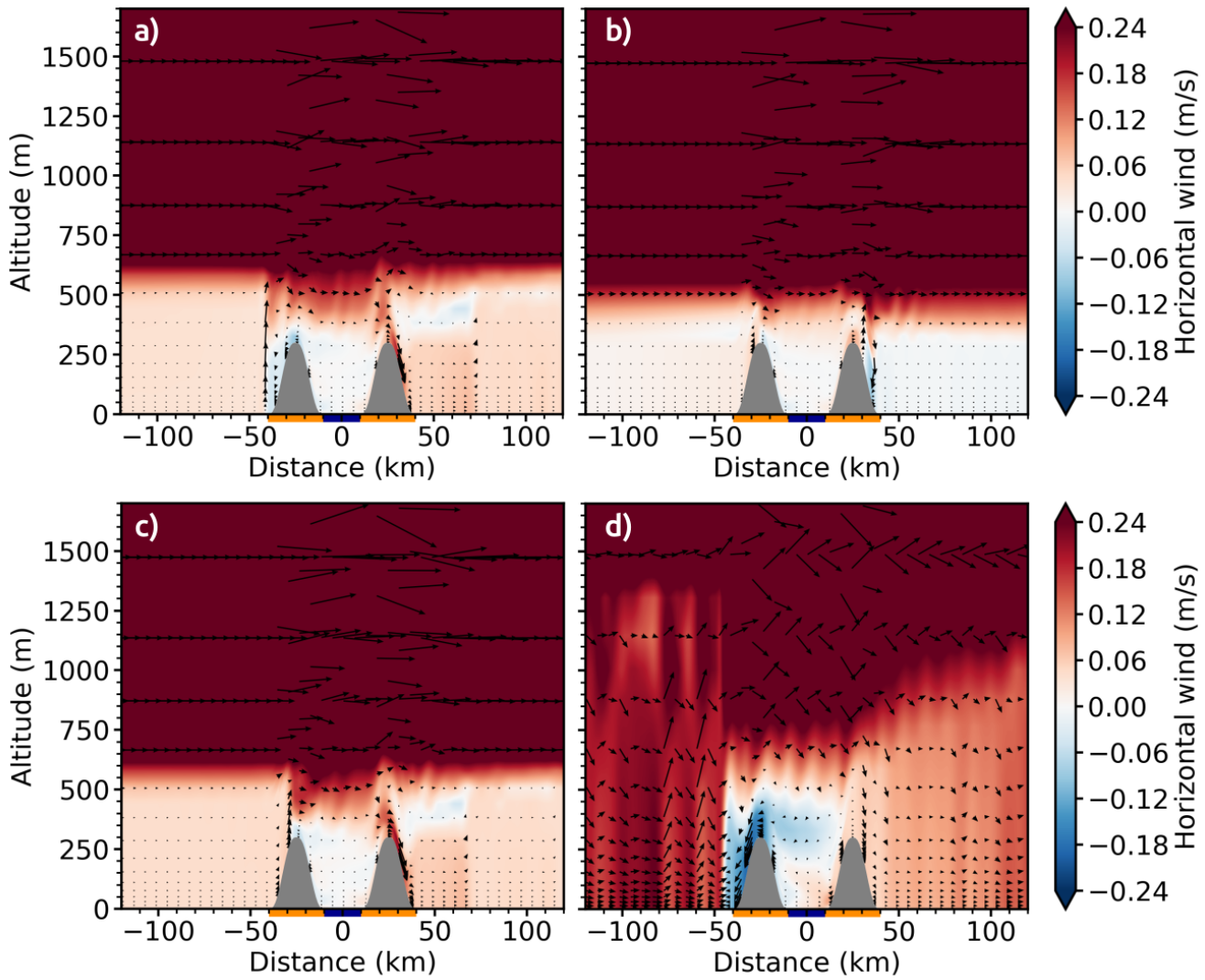

Figure 9. Horizontal wind at 2 a.m. at different seasons. (a) Autumn, (b) winter, (c) spring, and (d) summer. The black arrows represent the wind speed and direction to show the relative strength of the wind in the general circulation and close to the lake.

4. Conclusions and Perspectives

4.1. Conclusions

Using the mtWRF model and including SED and rampart properties, we report three main findings:

1. Around lakes near Titan's north pole, model simulations show the formation of lake breezes extending from the lake during the night due to the extremely stable atmospheric conditions and remaining closer to the lake during the day due to daytime turbulence. For instance, in autumn, in the case of a lake with a diameter of 20 km surrounded by ramparts (30 km wide and 300 m high), the maximum horizontal wind speed is around 0.04 m s^{-1} above the lake and around 0.2 m s^{-1} at the ramparts. The average latent heat flux over the lake is $\approx$0.39 W m^{-2}, which corresponds to a lake level change of -5.4 cm yr^{-1} (not including any possible recharge mechanisms by rain or subsurface supply).

2. Adding topography, varying the surface properties around the lakes of Titan or changing the season does not change the morphology of the atmospheric circulation around the lakes (lake breeze). However, it changes the intensity of the winds, the extent of the lake breeze, and the amount of methane evaporated.

In particular, adding topography around the lake decreases the amount of methane evaporated from the lake by approximately 10% due to slower winds above the lake ($\approx -30\%$). The addition of topography also increases the depth of the methane marine layer above the lake surface (from a few meters to a few tens of meters). Moreover, the extension of the lake breeze depends on the shape of the topography around the lake, varying from -20% to $+5\%$ in the cases studied here.

Among the surface properties investigated, only the surface roughness length (varied from 0.4 to 40 cm) has a significant impact on the lake breeze and the methane evaporation. For instance, the maximum surface wind speed decreases by 50% with a higher roughness at the ramparts. The effects of the albedo and the thermal inertia are negligible, according to our results.

At different seasons, the evaporation rate varies between 4.5 cm yr^{-1} in winter and 13 cm yr^{-1} in summer. These values are smaller than previous estimates (G. Mitri et al. 2007; A. Chatain et al. 2022).

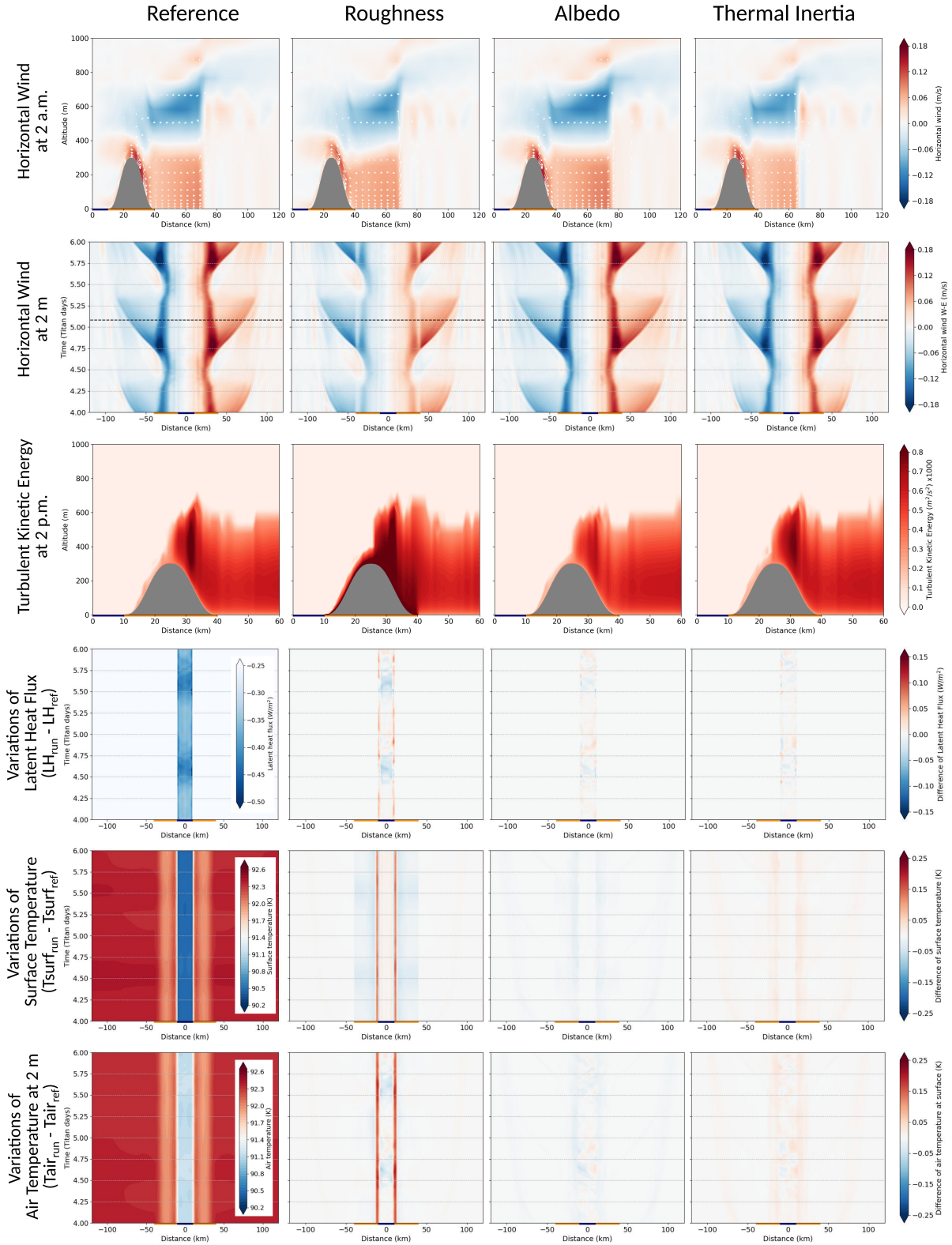

Figure 10. Effect of the surface properties of the ramparts on the lake breeze (winds, methane, temperature, and turbulence). We compare the reference simulation (in which ramparts have the same surface properties as the rest of the land) with the high-roughness case (see Section 3.3.1), the high-albedo case (see Section 3.3.2), and the high-thermal-inertia case (see Section 3.3.3). Row 1: horizontal wind at 2 a.m. Row 2: horizontal wind evolution at 2 m (the horizontal dashed lines show the location of the slices presented in Row 1). Row 3: TKE at 2 p.m.. Row 4: difference of latent heat flux compared to the reference (positive means more evaporation). Row 5: difference of surface temperature compared to the reference. Row 6: difference of air temperature at 2 m above the surface compared to the reference.

3. Without a lake, upslope winds are present day and night, with the strongest updrafts appearing at the end of the afternoon ($\approx$5 mm s^{-1}). These slope winds are created by a difference of net infrared flux at the surface. The simulation was performed at 74°N and at the autumnal equinox. Slope winds might be different at other seasons and could be explored in future works.

4.2. Perspectives

This work raises several questions:

On the possibility of forming waves. Waves are one of the main hypotheses to explain the "magic islands" that appeared on Ligeia Mare (J. D. Hofgartner et al. 2016). J. D. Hofgartner et al. (2016) predict that the minimum wind needed to form waves is $1.4\,\mathrm{m\,s^{-1}}$. However, our results are well under this value for all the simulations we performed in this work (1 order of magnitude). Surface winds of more than $1.4\,\mathrm{m\,s^{-1}}$ could appear in specific situations, maybe with a topography that favors wind channels, above a larger lake or sea, or due to 3D geometric effects (see A. Chatain et al. 2024).

On the mechanisms to form ramparts. Our simulations suggest that the lake breeze is a diurnally persistent feature. This leads us to consider an alternative or complementary mechanism that could explain the formation of the ramparts. The wind flowing from the lake could carry methane-coated aerosols with different properties than the usual aerosols deposited at the surface. These aerosols could accumulate at the lakeshore to form ramparts.

On the methane cycle in general: future studies. Here we focus on SED lakes at the north pole of Titan and on the effect of ramparts. This specific object of study is part of the larger objective of understanding the tropospheric methane cycle on Titan, which is an interesting analog to Earth's hydrological cycle.

1. In our study, we tested a situation with a lake and a situation with dry land. It would be interesting to simulate a wetland. Indeed, we do not know what the characteristic humidity of the surface (J. L. Mitchell & J. M. Lora 2016) is, and some studies suggest evidence for widespread wetlands at low-elevation terrains (C. D. Neish & R. D. Lorenz 2014).
2. One of the main limitations of our model is the absence of a microphysics scheme, thereby preventing the condensation of methane. We do not reach saturation conditions in our study; however, clouds have been reported to form close to lakes and seas at the north pole (M. E. Brown et al. 2009a). Thus, a next step will be to add a microphysics scheme and study the formation of methane clouds and methane storms.

Acknowledgments

Carbon Footprint. This worked required approximately 500 hr computation on a local server. We estimate the associated carbon emissions to be of the order of magnitude of $10\,\mathrm{kgCO_{2e}}$, using the Labos1point5 platform for emission factors (Labos1point5 2025), and multiplying by the ratio of US/France carbon intensity of electricity generation (Energy Institute 2025). It was also associated with approximately $2\,\mathrm{tCO_{2e}}$ for work travel.

Funding. E.M. received funding from the Ecole Normale Supérieure de Lyon. A.C. has received funding for this project from the European Union's Horizon 2020 research and innovation program under the Marie Sklodowska-Curie grant agreement No. 101022760. S.R. and A.S. are grateful for the support from the NASA Solar System Workings Program under grant #80NSSC22K1378. S.R. received additional support from the JHU/APL Dragonfly Mission project.

Data. The authors thank J. Lora for providing the initial profiles of temperature, pressure, methane, and winds, from the TAM global circulation model (J. M. Lora et al. 2015).

Supporting Data

The supporting data are available on Zenodo: doi:10.5281/zenodo.14833640. It contains

1. A list of the simulations,
2. The simulations input and output files,
3. The postprocessing Python codes to plot figures from the outputs,
4. Gifs to visualize the horizontal and vertical wind in the reference simulation, and
5. Tables of latent heat flux and winds (mentioned at the beginning of Section 3).

Appendix A
Impact of New Emissivity Values

In A. Chatain et al. (2022), the surface emissivity was set to 0.9 everywhere. In this work, we adapted the emissivity to the values estimated in the scientific literature, i.e., 0.99 for the lake and 0.95 for the land (see Section 2.1).

Figure 11 shows that the surface temperature is decreased when we increase the emissivity at the land and at the lake. The overall shape of the lake breeze remains the same, even though the breeze extends farther ($\approx +10\,\mathrm{km}$, being around $+10\%$). One of the main changes is the stability of the atmosphere: the TKE obtained in the new configuration is fainter (see the last two rows of Figure 11), and the PBL height is lower ($\approx -30\%$). Increasing the emissivity of the lake from 0.95 to 0.99 further lowers the temperature of the lake ($\approx -0.15\,\mathrm{K}$) and of the land close to the lake. It also decreases the evaporation from the lake, lowering the latent heat flux of around 25%.

Indeed, a higher emissivity causes a larger outgoing infrared flux from the surface. As a result, the net infrared flux at the surface is lower, and the temperature decreases until it reaches a new equilibrium. The colder surface also cools the air just above by sensible heat flux. Thus, the air above the surface is less buoyant, and the atmosphere is more stable in the PBL than in the case with a low emissivity. Consequently, the turbulence is fainter, and the PBL is less high. Moreover, the latent heat flux depends on the temperature (through the saturation mixing ratio). As a result, the lower temperature at the lake reduces the evaporation.

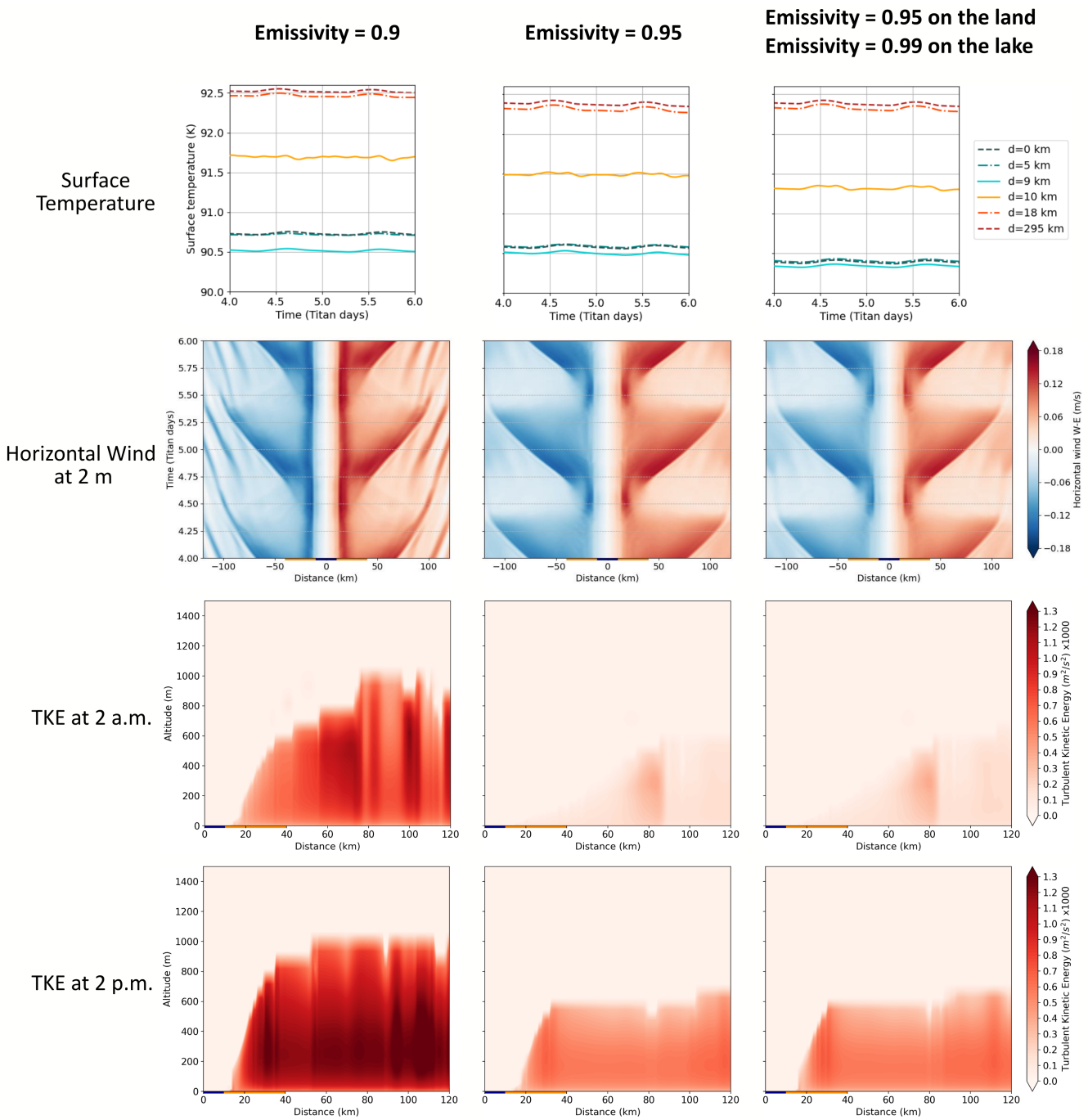

Figure 11. Comparison between the former emissivity (0.9, left) and the new one (0.99 over the lake and 0.95 over the land, right). The simulation shown in the middle is an intermediate case, with the emissivity set to 0.95 over the lake and the land. Rows, from top to bottom: surface temperature, horizontal wind at 2 m above the surface, TKE at 2 a.m., and TKE at 2 p.m.

Appendix B
Multiple Lakes Scenario

At the north pole of Titan, the lakes are often close to other lakes. To investigate the impact of grouped lakes on the local circulation, we make a simulation with two lakes separated by a rampart and surrounded by ramparts. We observe that the lake breezes of the lakes merge (Figure 12(a)). Moreover, some methane vapor is accumulated above the rampart between both lakes, increasing the relative humidity there (Figure 12(b)).

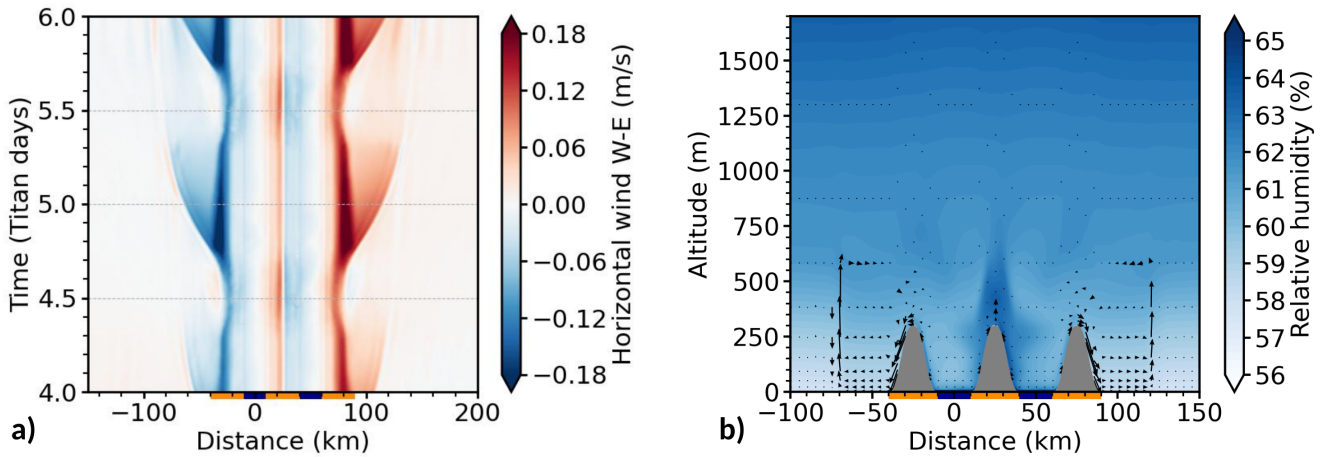

Figure 12. (a) Horizontal wind at 2 m above the surface. (b) Relative humidity at 2 a.m.

ORCID iDs

Enora Moisan https://orcid.org/0000-0002-2352-534X
Audrey Chatain https://orcid.org/0000-0002-2252-3254
Scot Rafkin https://orcid.org/0000-0001-7464-1319
Alejandro Soto https://orcid.org/0000-0002-2333-0307
Shannon MacKenzie https://orcid.org/0000-0002-1658-9687
Aymeric Spiga https://orcid.org/0000-0002-6776-6268

References

Arya, P. S. 2001, Introduction to Micrometeorology (Amsterdam: Elsevier), 448
Baciocco, C. 2021, The Impact of Improved Surface Boundary Conditions on Titan's Climate Patterns, BA thesis, Yale Univ. https://earth.yale.edu/sites/default/files/2025-08/Baciocco_thesis.pdf
Birch, S., Hayes, A., Lopes, R., et al. 2018, Raised Rims around Titan's Small Lakes, COSPAR Scientific Assembly, 42, B5.2–30–18
Birch, S. P. D., Hayes, A. G., Dietrich, W. E., et al. 2017, Geomorphologic Mapping of Titan's Polar Terrains: Constraining Surface Processes and Landscape Evolution, Icar, 282, 214
Birch, S. P. D., Hayes, A. G., Poggiali, V., et al. 2019, Raised Rims around Titan's Sharp-edged Depressions, GeoRL, 46, 5846
Blackadar, A. K. 1979, High-resolution Models of the Planetary Boundary Layer, Adv. Environ. Sci. Eng., 1, 50
Brouwer, G. E., Schurmeier, L. R., & Fagents, S. A. 2024, An Endogenic Origin for Titan's Rampart Craters: Assessment of Explosion Mechanisms, JGRE, 129, e2024JE008459
Brown, M. E., Schaller, E. L., Roe, H. G., et al. 2009a, Discovery of Lake-effect Clouds on Titan, GeoRL, 36, L01103
Brown, M. E., Smith, A. L., & Chen, C. 2009b, Discovery of FOG at the South Pole of Titan, ApJL, 706, L110
Chatain, A., Rafkin, S. C. R., Soto, A., et al. 2024, The Impact of Lake Shape and Size on Lake Breezes and Air-Lake Exchanges on Titan, Icar, 411, 115925
Chatain, A., Rafkin, S. C. R., Soto, A., Hueso, R., & Spiga, A. 2022, Air–Sea Interactions on Titan: Effect of Radiative Transfer on the Lake Evaporation and Atmospheric Circulation, PSJ, 3, 232
Dudhia, J. 1996, A Multi-layer Soil Temperature Model for MM5, in The Sixth PSU/NCAR Mesoscale Model Users' Workshop, 22
Energy Institute 2025, Statistical Review of World Energy (2024), Carbon Intensity of Electricity Generation 2025, Energy Institute https://www.energyinst.org/statistical-review/home
Farina, S., & Zardi, D. 2023, Understanding Thermally Driven Slope Winds: Recent Advances and Open Questions, BoLMe, 189, 5
Faulk, S. P., Mitchell, J. L., Moon, S., & Lora, J. M. 2017, Regional Patterns of Extreme Precipitation on Titan Consistent with Observed Alluvial Fan Distribution, NatGe, 10, 827
Garratt, J. R. 1977, Aerodynamic Roughness and Mean Monthly Surface Stress over Australia (Melbourne: CSIRO)
Hatchett, B. J. , Kaplan, M. L., Nicholas, N. J. , Smith, C. M., & Nelson, K. 2020, Slope Winds, in Encyclopedia of Wildfires and Wildland-Urban Interface (WUI) Fires, ed. L. M. Samuel (Berlin: Springer), 922
Hayes, A., Aharonson, O., Callahan, P., et al. 2008, Hydrocarbon Lakes on Titan: Distribution and Interaction with a Porous Regolith, GeoRL, 35, L09204
Hayes, A. G. 2016, The Lakes and Seas of Titan, AREPS, 44, 57
Hayes, A. G., Birch, S. P. D., Dietrich, W. E., et al. 2017, Topographic Constraints on the Evolution and Connectivity of Titan's Lacustrine Basins, GeoRL, 44, 11745
Hayes, A. G., Lorenz, R. D., & Lunine, J. I. 2018, A Post-Cassini View of Titan's Methane-based Hydrologic Cycle, NatGe, 11, 306
Hofgartner, J. D., Hayes, A. G., Lunine, J. I., et al. 2016, Titan's "Magic Islands": Transient Features in a Hydrocarbon sea, Icar, 271, 338
Janjić, Z. I. 1994, The Step-mountain Eta Coordinate Model: Further Developments of the Convection, Viscous Sublayer, and Turbulence Closure Schemes, MWRv, 122, 927
Janjić, Z. I. 1996, The Surface Layer Parameterization in the NCEP Eta Model 4.16, World Meteorological Organization, Working Group on Numerical Experimentation, Commission for Atmospheric Sciences, World Climate Research Program
Janjić, Z. I. 2001, Nonsingular Implementation of the Mellor-Yamada Level 2.5 Scheme in the NCEP Meso Model 437, National Centers for Environmental Prediction https://repository.library.noaa.gov/view/noaa/11409
Jennings, D. E., Cottini, V., Nixon, C. A., et al. 2011, Seasonal Changes in Titan's Surface Temperatures, ApJL, 737, L15
Labos1point5 2025, 1point5 | Applications, https://apps.labos1point5.org/documentation
Lebonnois, S., Schubert, G., Forget, F., & Spiga, A. 2018, Planetary Boundary Layer and Slope Winds on Venus, Icar, 314, 149
Le Gall, A., Malaska, M. J., Lorenz, R. D., et al. 2016, Composition, Seasonal Change, and Bathymetry of Ligeia Mare, Titan, Derived from its Microwave Thermal Emission, JGRE, 121, 233
Lettau, H. 1969, Note on Aerodynamic Roughness-parameter Estimation on the Basis of Roughness-Element Description, JApMe, 8, 828
Lopes, R. M. C., Malaska, M. J., Solomonidou, A., et al. 2016, Nature, Distribution, and Origin of Titan's Undifferentiated Plains, Icar, 270, 162
Lora, J. M., Battalio, J. M., Yap, M., & Baciocco, C. 2022, Topographic and Orbital Forcing of Titan's Hydroclimate, Icar, 384, 115095
Lora, J. M., Lunine, J. I., & Russell, J. L. 2015, GCM Simulations of Titan's Middle and Lower Atmosphere and Comparison to Observations, Icar, 250, 516
Lorenz, R. D. 2021, An Engineering Model of Titan Surface Winds for Dragonfly Landed Operations, AdSpR, 67, 2219
MacKenzie, S. M., Barnes, J. W., Hofgartner, J. D., et al. 2019a, The Case for Seasonal Surface Changes at Titan's Lake District, NatAs, 3, 506
MacKenzie, S. M., Lora, J. M., & Lorenz, R. D. 2019b, A Thermal Inertia Map of Titan, JGRE, 124, 1728
Mesinger, F. 1993, Forecasting Upper Tropospheric Turbulence within the Framework of the Mellor-Yamada 2.5 Closure in Research Activities in Atmospheric and Oceanic Modelling, 4.28CAS/JSC WGNE 1993

Michaelides, R. J., Hayes, A. G., Mastrogiuseppe, M., et al. 2016, Constraining the Physical Properties of Titan's Empty Lake Basins using Nadir and Off-Nadir Cassini RADAR Backscatter, Icar, 270, 57
Mitchell, J. L., & Lora, J. M. 2016, The Climate of Titan, AREPS, 44, 353
Mitri, G., Lunine, J. I., Mastrogiuseppe, M., & Poggiali, V. 2019, Possible Explosion Crater Origin of Small Lake Basins with Raised Rims on Titan, NatGe, 12, 791
Mitri, G., Showman, A. P., Lunine, J. I., & Lorenz, R. D. 2007, Hydrocarbon Lakes on Titan, Icar, 186, 385
Monin, A. S., & Obukhov, A. M. 1954, Basic Laws of Turbulent Mixing in the Surface Layer of the Atmosphere, Contrib. Geophys. Inst. Acad. Sci. USSR, 151, e187
Moses, J. I., Allen, M., & Yung, Y. L. 1992, Hydrocarbon Nucleation and Aerosol Formation in Neptune's Atmosphere, Icar, 99, 318
Neish, C. D., & Lorenz, R. D. 2014, Elevation Distribution of Titan's Craters Suggests Extensive Wetlands, Icar, 228, 27
Rafkin, S. C. R., & Soto, A. 2020, Air-Sea Interactions on Titan: Lake Evaporation, Atmospheric Circulation, and Cloud Formation, Icar, 351, 113903
Savijärvi, H., & Siili, T. 1993, The Martian Slope Winds and the Nocturnal PBL Jet, JAtS, 50, 77
Skamarock, C., Klemp, B., Dudhia, J., et al. 2008, A Description of the Advanced Research WRF Version 3 TN–475+STR, National Center for Atmospheric Research
Solomonidou, A., Le Gall, A., Malaska, M. J., et al. 2019, The Raised Ramparts Around Titan's Northern Lakes, EGU General Assembly, 21, 9493
Solomonidou, A., Le Gall, A., Malaska, M. J., et al. 2020, Spectral and Emissivity Analysis of the Raised Ramparts around Titan's Northern Lakes, Icar, 344, 113338
Stofan, E. R., Elachi, C., Lunine, J. I., et al. 2007, The Lakes of Titan, Natur, 445, 61
Tokano, T., Ferri, F., Colombatti, G., Mäkinen, T., & Fulchignoni, M. 2006, Titan's Planetary Boundary Layer Structure at the Huygens Landing Site, JGRE, 111, E08007
Wood, C. A., Mitchell, K., Radebaugh, J., et al. 2006, Lake-filled Volcanic Calderas of Titan, AAS/DPS Meeting, 38, 52.06
Wood, C. A., & Radebaugh, J. 2020, Morphologic Evidence for Volcanic Craters Near Titan's North Polar Region, JGRE, 125, e2019JE006036
Yu, X., Yu, Y., Garver, J., Zhang, X., & McGuiggan, P. 2024, The Fate of Simple Organics on Titan's Surface: A Theoretical Perspective, GeoRL, 51, e2023GL106156